AFRL-RV-PS-
TM-2014-0001

A MODEL OF MEDIAN AURORAL ELECTRON FLUX DEDUCED FROM HARDY 2008 MODEL PROBABILITY DENSITY MAPS

Chin S. Lin, et al.

01 November 2013

Technical Memorandum

AIR FORCE RESEARCH LABORATORY
Space Vehicles Directorate
3550 Aberdeen Ave SE
AIR FORCE MATERIEL COMMAND
KIRTLAND AIR FORCE BASE, NM 87117-5776

DTIC COPY

NOTICE AND SIGNATURE PAGE

AFRL-RV-PS-TM-2014-0001 HAS BEEN REVIEWED AND IS APPROVED FOR PUBLICATION IN ACCORDANCE WITH ASSIGNED DISTRIBUTION STATEMENT.

//SIGNED//	//SIGNED//
Dr. Cassandra G. Fesen	Edward J. Masterson, Colonel, USAF
Program Manager, AFRL/RVBX	Chief, Battlespace Environment Division

REPORT DOCUMENTATION PAGE

Form Approved
OMB No. 0704-0188

1. REPORT DATE *(DD-MM-YYYY)*	**2. REPORT TYPE**	**3. DATES COVERED** *(From - To)*
01-11-2013	Technical Memorandum	01 Jan 2013 – 31 Oct 2013

4. TITLE AND SUBTITLE
A Model of Median Auroral Electron Flux Deduced from Hardy 2008 Model Probability Density Maps

5a. CONTRACT NUMBER

5b. GRANT NUMBER

5c. PROGRAM ELEMENT NUMBER
62601F

6. AUTHOR(S)
C. S. Lin, P. F. Lei,* and W. J. Burke

5d. PROJECT NUMBER
1010

5e. TASK NUMBER
PPM00005184

5f. WORK UNIT NUMBER
EF004415

7. PERFORMING ORGANIZATION NAME(S) AND ADDRESS(ES)
Air Force Research Laboratory
Space Vehicles Directorate
3550 Aberdeen Avenue SE
Kirtland AFB, NM 87117-5776

*Boston College
140 Commonwealth Ave.
Chestnut Hill, MA 02467

8. PERFORMING ORGANIZATION REPORT NUMBER
AFRL-RV-PS-TM-2014-0001

9. SPONSORING / MONITORING AGENCY NAME(S) AND ADDRESS(ES)

10. SPONSOR/MONITOR'S ACRONYM(S)
AFRL/RVBX

11. SPONSOR/MONITOR'S REPORT NUMBER(S)

12. DISTRIBUTION / AVAILABILITY STATEMENT

Approved for public release; distribution is unlimited. (377ABW-2013-0977 dtd 06 Nov 2013)

13. SUPPLEMENTARY NOTES
In-house research performed under IONO Program/Ionospheric Impacts on RF Systems

14. ABSTRACT

The Hardy auroral precipitation flux model has been extensively used for modeling high latitude phenomena and space weather operation since its initial development in 1985. The original Hardy model (referred here as H-85 model) specifies the average pattern of auroral electron precipitation as a function of geomagnetic latitude, magnetic local time and magnetic activity Kp index. The H-85 model has recently been extended into a probability model in 2008 with a much larger collection of new DMSP observations since 1985. The upgraded Hardy model, referred here as H-08, turns out to be a large database and lacks functional representation. The purpose of this paper is to present an approach to functionally represent the H-08 model. We reduced median auroral fluxes from the H-08 model probability maps, and conducted a regression analysis to fit the median auroral fluxes using real spherical harmonics. We derived a reduced model of median auroral fluxes named as H-08MV to distinguish it from the earlier models. The developed functional representation will greatly enhance usefulness of the new Hardy model for space weather prediction.

15. SUBJECT TERMS
Auroral flux model, auroral oval boundary, auroral electron flux

16. SECURITY CLASSIFICATION OF:			**17. LIMITATION OF ABSTRACT**	**18. NUMBER OF PAGES**	**19a. NAME OF RESPONSIBLE PERSON**
a. REPORT	**b. ABSTRACT**	**c. THIS PAGE**			Dr. Cassandra G. Fesen
Unclassified	Unclassified	Unclassified	Unlimited	26	**19b. TELEPHONE NUMBER** *(include area code)*

This page is intentionally left blank.

Table of Contents

List of Figures

1. Introduction

Auroral oval boundary has been considered a critical requirement for the DMSP mission and space situation awareness. The auroral boundary specification supports requirements for global situational awareness of geomagnetic activity. The operational DOD ionosphere specification model uses both boundaries as key inputs. Another well known example of auroral oval boundary utility is the high latitude radar surveillance systems where the auroral boundary location is used to help discriminate radar clutter from images of projectile objects. HF and radio systems near the auroral zone are greatly affected by auroral precipitation which causes enhanced ionization in the ionospheric E-region. Both the equatorward and poleward boundaries of the auroral zone are operationally derived from particle flux measurements acquired by DMSP satellites.

The Hardy Auroral electron flux model has been very useful for modeling high latitude auroral oval boundary since its initial development in 1985 by Hardy et al. (1985) using DMSP particle flux data. The original Hardy model referred to as H-85 here is extensively used for studying auroral precipitation phenomena in the space weather community. It was upgraded in 2008 by expanding the amount of DMSP particle spectrometer data used in the analysis (Hardy et al., 2008). The upgraded Hardy model, referred here as H-08, turns out to be a large database and lacks functional representation. As a consequence no utility has been developed for it yet. To explore its utilities, we attempted to derive a functional representation. In our first attempt we reduced median auroral fluxes from the H-08 model, and conducted a regression analysis to fit the median auroral fluxes using real spherical harmonics functions. The reduced model of median auroral fluxes we obtained is named as H-08MV to distinguish it from the earlier models. The purpose of this report is to describe our preliminary results. We first review the H-85 and H-08 models in the next section. Next in Section 3 we compare auroral oval boundaries as determined by these two Hardy models. Section 4 describes the regression analysis using real spherical harmonics. In the Appendix we list tables of expansion coefficients in the functional representation. Finally concluding remarks are given in Section 5.

The Hardy Auroral electron flux model (H-85) currently used in the space weather community was originally derived from precipitating particle measurements made by the Special Sensor for Precipitating Particles, version 4 (SSJ4) electrostatic analyzers flown on the F6 and F7 satellites of the Defense Meteorological Satellite Program (DMSP) (Hardy *et al*, 1985; Hardy *et al.*, 1987). A total of 2 years of ion and electron data (1983 data for F6 and 1984 data for F7) were used to develop the H-85. The SSJ/4 analyzers measured electron and ion spectra in the local satellite zenith direction once per second over 20 channels spanning an energy range from 30 eV to 30 keV. Statistical hemispheric particle precipitation maps were created for a range of different magnetospheric activity levels defined by the Kp index. The particle precipitation map is defined in the coordinate of corrected geomagnetic latitude (MLat) and magnetic local time (MLT). The high-latitude region grid was defined by 30 zones in MLat between 50^o and 90^o and 48 half-hour zones in MLT. Each latitude zone was 2^o wide between 50^o and 60^o and 1^o wide between 60^o and 80^o latitude. Measurements in each of the energy channels were accumulated to build a one-second average of the differential number flux spectra for each bin. The resulting average spectra were then extrapolated to 100 keV and integrated over energy to yield integral number flux and integral energy flux. The differential

number flux spectra were assumed to be isotropic in the integration. The average energy was calculated as ratio of integral energy flux to integral number flux. Figure 1 produced by the AF-Geospace Software (Hilmer, 2010) illustrates the precipitating electron energy flux map in the Northern hemisphere for Kp = 3.

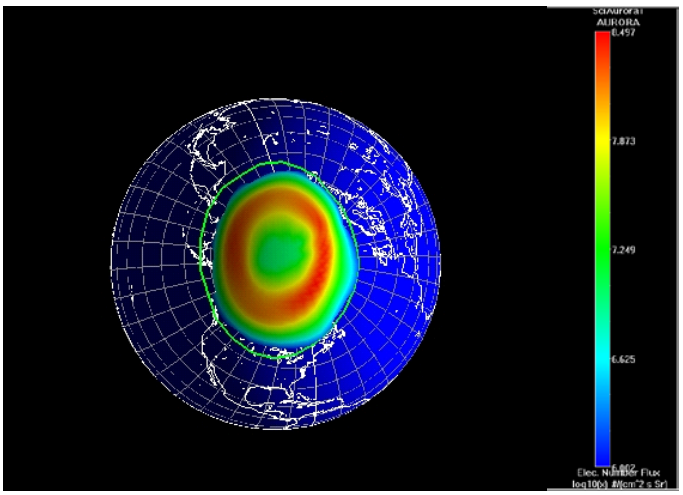

Figure 1. An example of the precipitating electron energy flux map in the Northern hemisphere for Kp=3 produced by AF-Geospace software. *The green line specifies the auroral oval boundary.*

The H-85 model was upgraded to H-08 in 2008 by re-analyzing historical DMSP particle spectrometer data from 1983 to 2005 from a series of 9 DMSP satellites (Hardy *et al.*, 2008). The statistical study was conducted using more than 600 million energetic electron spectra measured by the SSJ4 sensor to obtain total number fluxes J_{tot} in the unit of #/cm^2-s-sr and energy fluxes JE_{tot} in the unit of keV/cm^2-s-sr. As a big database the H-08 model is difficult to use. It does not have explicit algorithm for calculating the auroral oval boundary. It divides the ranges of total number flux and average energy in logarithmic scale into 26X26 probability maps for each bin of Kp, MLat, and MLT. The H-08 model has Kp integer values from 0 to 9, MLat from 43 to 89 and MLT from 0 to 23.

Some improvements over the H-85 model are:

(1) H-08 divides data into bins 1° by 1 hr in magnetic latitude and magnetic local time, respectively. The H-08 latitude bin is 1^o from geomagnetic latitude 50^o to the pole, whereas the H-85 latitude bin is 1^o wide only between 60^o and 80^o. However the original H-85 model has a magnetic local time bin width ½ hour smaller than H-08.

(2) H-08 provides probabilities of encountering different levels of total number flux J_{tot}, total energy flux JE_{tot} and average energy ($E_{ave} = JE_{tot}/ J_{tot}$), whereas no probability statistics are available from H-85. H-08 demonstrates that within all MLat-MLT bins probabilities for encountering different levels of J_{tot}, $JE_{tot,}$ and E_{ave} are lognormal distributed. Often more than one population can be found.

(3) Both the H-85 and H-08 models represent data according to the level of the Kp index. The H-85 electron flux characteristics were determined for each whole number value of Kp from 0 to 5 and for Kp > 6-. The H-08 model specifies the electron flux probability for the whole Kp range from 0 to 9. However the statistics are poor for Kp > 8 because of its small sampling size.
(4) The methodologies used in the two Hardy models are different. The H-85 model was developed by first taking the average number flux spectra in each energy bin and then integrating them to obtain J_{tot} and JE_{tot}. In contrast Hardy *et al.* (2008) integrated first number and energy fluxes over energy and then performed statistics to derive their probability.

Figure 2 illustrates a representative output of the H-08 model for the evening (20 MLT) sector at auroral (72^o, 69^o, and 65^o) and subauroral (60^o) magnetic latitudes. Contours of constant probability densities are plotted as functions of log JE_{tot} (abscissa) and log E_{ave} (ordinate), where log is the 10-base logarithmic. With these coordinates a single lognormal distribution would appear as a circular region with an intensity peak at the center. As indicated in Figure 2, probability distributions at auroral latitudes were represented by multiple lognormal distributions in different ranges of E_{ave} and JE_{tot}. The top panel of Figure 2 (MLat = 72^o) shows clear evidence of two populations that are distinct in both E_{ave} and JE_{tot}. Peaks occur in E_{ave} near 0.2 and 1 keV. In the subauroral example (bottom panel, 60^o), E_{ave}-JE_{tot} characteristics are those of conjugate photoelectrons at E_{ave} < 100 eV that were encountered during ~20% of the DMSP orbits. The third panel (65^o) also shows clear conjugate photoelectron population at the lower left corner.

From the occurrence probability maps such as those shown in the first column of Figure 2, the H-08 model can be used to yield the average-energy-flux probability PF(log JE_{tot}) that specifies the probability of detecting average auroral energy flux at the level of JE_{tot} in an MLat-MLT and Kp bin. The average-energy-flux probability PF(log JE_{tot}) is obtained by integrating the model lognormal distributions over E_{ave}. The second column in Figure 2 illustrates PF(log JE_{tot}) as a function of log JE_{tot} corresponding to the first column. The average-energy-flux probability PF(log JE_{tot}) is comprised of several components as plotted in colored lines. Purple, yellow and green traces indicate fitted distributions of the primary, secondary and tertiary populations, respectively. Blue lines are sums of fitted probability distributions. Red curves represent measured probability distributions. The top and third panels indicate that PF (log JE_{tot}) is represented by bimodal lognormal probability distributions. The second and fourth panels on the other hand suggest PF(log JE_{tot}) is dominated by a single component. Similarly the H-08 model can be used to specify the probability for detecting average energy at a specified level of E_{ave} (Figure 2, right column).

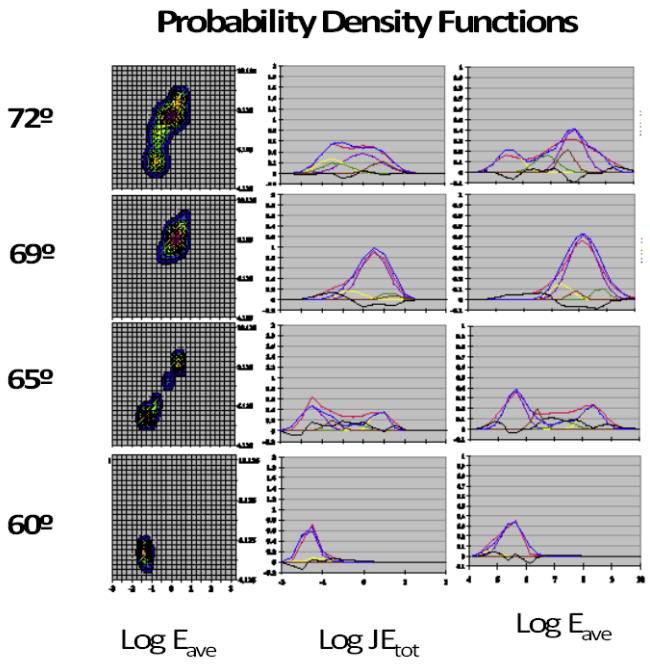

Figure 2. Four representative samples of the probability distributions output from the Hardy H-08 model along the MLT = 20 meridian for Kp = 3.
Their magnetic latitudes are shown at the left side. Left column: contours of constant probability densities as functions of log JE_{tot} (abscissa) and log E_{ave} (ordinate). Middle column: average energy flux probability PF(log JE_{tot}) as a function of log JE_{tot}. Right column: average-energy probability PF(log E_{ave}) as a function of log E_{ave}. (from Hardy et al. 2008). Red curves represent measured probability distributions. Purple, yellow and green traces indicate fitted distributions of the primary, secondary and tertiary populations, respectively. Blue lines are sums of fitted probability distributions.

2. Auroral Oval Boundary Model

The H-85 model can provide a map of auroral boundary at all longitudes for a given geomagnetic activity. It contains an algorithm to specify the equatorward auroral oval boundary. The auroral oval boundary algorithm is not based on the spatial map of model electron fluxes. Instead it was deduced from a separate statistics study [*Gussenhoven et al.*, 1981; *Gussenhoven et al.*, 1983]. The equatorward boundary was determined for each DMSP pass from latitudinal profiles of the electron integral number flux. A large number of DMSP boundary crossings (over 200,000 passes) in the interval 1983-1990 were included in the statistics [*Madden and Gussenhoven* 1990]. Because the auroral energy flux and boundary models are based on two independent statistical studies, the equatorward edge of the H-85 energy flux distribution is close to but do not always coincide with the auroral oval boundary determined in the model. For example the green line in Figure 1 that specifies the auroral oval

boundary from the model lies outside the area of electron precipitating fluxes. These boundaries would be closer with a different choice of threshold flux value.

The *Gussenhoven et al.* [6] regression analysis linearly fit the equatorward boundary versus the Kp index for 24 hourly sectors in MLT. The equatorward boundary Λ was expressed in a linear equation of Kp,

$$\Lambda = \Lambda_o + \alpha K_p \tag{1}$$

where Λ_o and α are the intercept and slope, respectively, for each magnetic local time bin. Figure 3 illustrates the variation of the auroral equatorward boundary Λ versus Kp in the 2300-2400 hour bin. This figure shows that Λ decreases from about 67^o when Kp = 1 to less than 55^o when Kp = 7.

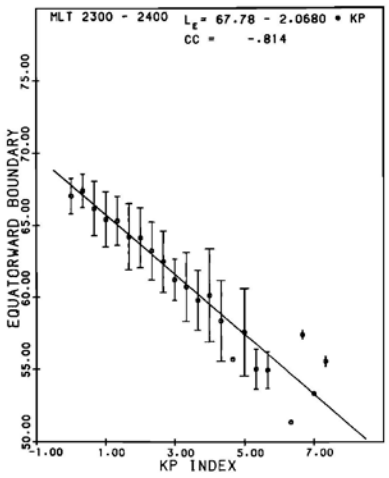

Figure 3. Mean values (solid line) and standard deviation (vertical bar) in each Kp bin as a function of Kp for the 2300-2400 MLT sector (from Gussenhoven *et al.* 1983).

Recently the equatorward boundary statistics have been updated in the AF-Geospace software with the extensive DMSP auroral particle data. Table A1 in Appendix A lists the updated values of Λ_o and α for 24 hourly sectors. Note that Table A1 contains regression coefficients for a few MLT bins that were originally unavailable in the original work of *Gussenhoven et al.* (1983).

Based on the H-85 auroral boundary model, Madden and Gussenhoven (1990) developed an auroral boundary index as the equivalent midnight boundary after removing local time variation. The temporal variation of the midnight auroral boundary index follows auroral activity and can be used to predict global changes in the auroral oval. It was demonstrated that the midnight auroral boundary index more accurately reflects magnetic activity than the Kp index at time scale much shorter than the Kp's three-hour increment (Madden and Gussenhoven, 1990).

As a big database the H-08 model is difficult to use. It does not have an explicit algorithm for calculating the auroral oval boundary. It divides the ranges of total number flux and average energy in logarithmic scale into 26X26 probability maps for each bin of Kp, MLat, and MLT. The H-08 model has Kp integer values from 0 to 9, MLat from 43 to 89 and MLT from 0 to 23.

Similar to *Gussenhoven et al.* (1983), we manually scanned the H-08 probability maps to determine the threshold value of MLat where the occurrence probability of detecting electron flux drops rapidly to zero. Specifically the two criteria for determining an auroral boundary were electron number flux greater than 10^7 #/cm^2-sec-sr and the encounter probability greater than 0.5. The low and high latitudinal boundaries were determined for each MLT and each Kp from 0 to 6. Due to insufficient coverage for Kp > 6 the probability maps do not have good statistics to yield a good average model of auroral boundary at Kp > 6. The magnetic latitudes of the auroral boundaries are fitted by sinusoidal functions of MLT for each Kp bin as

$$\Lambda_L = a_0 + \sum_{n=1}^{n=4} \left(a_n \cos\frac{n\pi x}{180} + b_n \sin\frac{n\pi x}{180} \right) \quad (2)$$

and

$$\Lambda_H = c_0 + \sum_{n=1}^{n=3} \left(c_n \cos\frac{n\pi x}{180} + d_n \sin\frac{n\pi x}{180} \right) \quad (3)$$

where Λ_L and Λ_H are the MLat of the low and high latitude boundary, respectively, and x is MLT expressed in degrees (x = 15*MLT). The Λ_L expansion coefficients a_n and b_n up to n = 4 harmonics are given in Appendix B (Table B1) for Kp from 0 to 6. Because the high latitude boundary Λ_H appears to vary gradually with MLT, Λ_H is fitted only up to n = 3 harmonics. Its coefficients c_n and d_n are listed in Appendix B (Table B2). From these tables the auroral boundary MLat for fractional Kp value can be specified by linearly interpolation.

Figure 4 compares the H-08 low latitude auroral boundary Λ_L determined from Equation (2) with the H-85 equatorward boundary Λ expressed in Equation (1) for Kp = 1, 3, and 5. This figure shows that Λ_L (solid line) is slightly lower than Λ (red triangle) in the 1000-1600 MLT hours. For other MLTs, Λ_L and Λ are about the same.

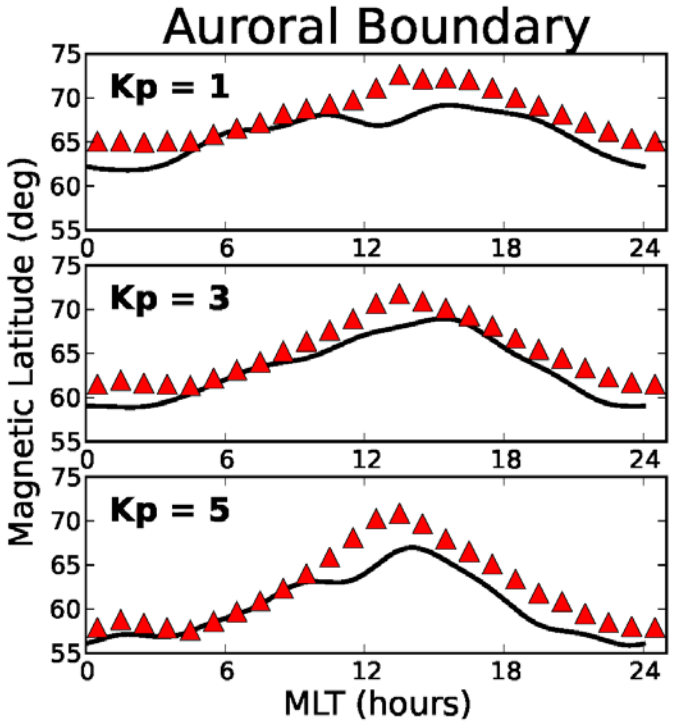

Figure 4. Comparison of auroral oval boundaries between the H-85 and H-08 models.

The solid line in each Kp panel represents the low latitude auroral boundary Λ_L determined from the H-08 probability maps. The H-85 equatorward auroral boundary from Equation (1) is plotted as solid triangle.

3. H-08 Median Values (H-08MV) Model

An auroral specification capability based on the H-08 model would have a wealth of statistical information that could potentially provide new and improved information. For instance more accurate confidence levels could be provided to system operators and better error estimates could be passed to models assimilating auroral fluxes. Here we discuss a first attempt to make the H-08 more accessible; this model was studied in the validation effort described in Section 5.

Since the H-08 model is a large database and lacks functional representation, no utility has been developed for it yet. To explore its utilities, we attempted to derive a functional representation of the H-08 model. We first determined the medians of PF(log JE_{tot}) and PF(log E_{ave}) for each MLat-MLT-Kp bin from their H-08 model occurrence probability maps, respectively. Figure 5 illustrates the obtained median energy flux log JE_{tot} as a function of MLat at MLT = 0 for Kp from 0 to 6.

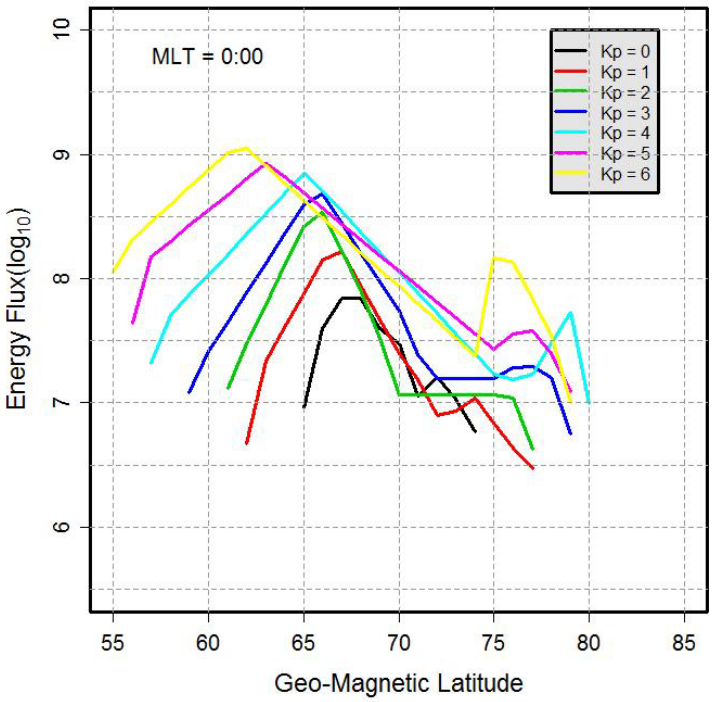

Figure 5. Median energy flux from the H-08MV model as a function of magnetic latitude at MLT = 0 for Kp from 0 to 6.

In order to expand log JE_{tot} and log E_{ave} in terms of spherical harmonics functions, we define a normalized variable θ between the lower and upper auroral boundaries (Λ_L and Λ_H) as

$$\theta = \frac{\pi(MLat - \Lambda_0)}{(\Lambda_H - \Lambda_L)} \tag{4}$$

where Λ_L is defined as (Λ_L + Λ_H)/2. Note that θ varies from -π/2 to π/2 as MLat varies from Λ_L to Λ_H. Similarly we define ϕ = πMLT/12 that varies from 0 to 2π to replace the MLT angle from midnight. For each Kp multivariate regression analysis was performed to fit median values of JE_{tot} and E_{ave} versus θ and ϕ, respectively, by real spherical harmonics $y_{lk}(\theta, \phi)$ (www.wikipedia.org) as:

$$JE_{tot}(\theta, \phi) = \sum_{l=0}^{l=4} \sum_{k=0}^{k=2l} C_{lk} y_{lk}(\theta, \phi) \tag{5}$$

and

$$E_{ave}(\theta, \phi) = \sum_{l=0}^{l=4} \sum_{k=0}^{k=2l} D_{lk} y_{lk}(\theta, \phi) \tag{6}$$

ϕ is MLT expressed as angle from midnight in radian, C_{lk} and D_{lk} are the expansion coefficients determined from regression analysis using up to 4th order real spherical harmonics y_{lk} functions (l from 0 to 4, and k from 0 to 2l). Tables C1 and C2 in Appendix C list the regression coefficients C_{lk} and D_{lk}, respectively, for Kp = 0 to 6. The function representation of Equations (5) and (6) along with lookup tables of C_{lk} and D_{lk} constitute the reduced model of median auroral fluxes and energy, which we named it the H-08 Median Value (H-08MV)

model to distinguish it from the earlier Hardy models. The H-08MV representation allows straightforward calculation of median auroral energy flux and median energy at given MLat and integer Kp. Interpolation is applied for fractional Kp. A Fortran computer code for the H-08MV model is available from the authors upon request.

Figure 6 shows contour plots of the median auroral energy flux and median energy for Kp = 0 to 6. The H-08MV contours indicate that the low latitude boundary of auroral electron precipitation extends from 70^o to 55^o as Kp increases from 0 to 6. Both JE_{tot} and E_{ave} medians increase with Kp.

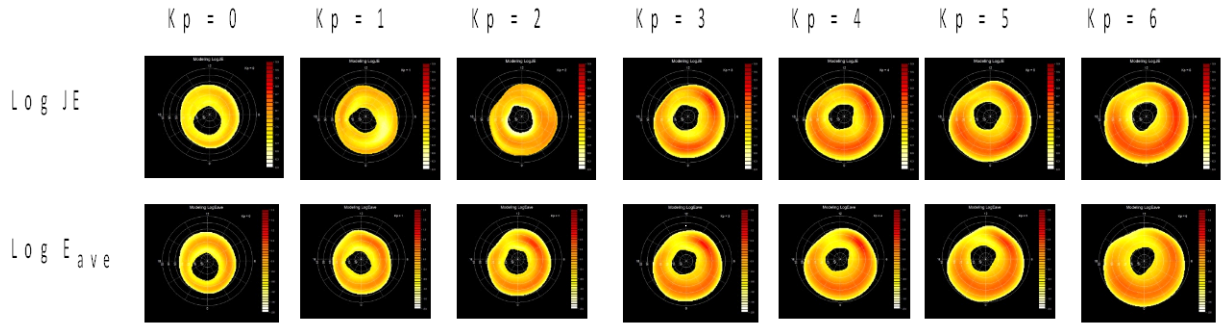

Figure 6. Contour plots of the median auroral energy flux and median energy from the H-08MV model for Kp = 0 to 6.

4. Discussion

The H-85 and H-08MV models have been recently examined in the validation study of auroral oval models by Lane (2012) in which several available models specifying the auroral oval boundary were validated with DMSP satellite measurements. Lane (2012) represented the equatorward boundary as the location at which energy flux measured by DMSP satellites exceeded a fixed threshold of 0.4 erg/cm2/s. The observed auroral boundary locations were compared with predictions from H-85, H-08MV, Ovation Prime model, Space Weather Modeling Framework model, and Assimilative Mapping of Ionospheric Electrodynamics (AMIE) model.

The validation study used data obtained from 3 DMSP satellite passes during a total of 28 days in the period of 2000 to 2008. These dates included 13 days covering five prominent geomagnetic storms and 15 days with low and moderate Kp values. A total of 6,297 DMSP satellite passes were included in this study. Unfortunately due to limited data availability no validation study was performed for critical local times from 22 to 03 MLT.

Lane (2012) studied the model prediction efficiency (PE) by evaluating the coefficient of efficiency defined as

$$PE = 1 - \frac{\sum_{i=1}^{N}(y_i - x_i)^2}{\sum_{i=1}^{N}(y_i - \bar{y})^2} \quad (7)$$

where N is the number of data points, y_i is the i-th data point, $\bar{y}$ is the mean of the data set, and x_i is the model prediction value correspond to y_i. The PE score measures the percentage of variance in the observed DMSP data captured by the model. Thus, a PE score of 1 indicates perfect prediction by the model. An efficiency of 0 ($PE = 0$) indicates that the model prediction is as accurate as the mean of the observed data.

Lane (2012) found the Ovation Prime model to have the highest overall prediction efficiency score (PE = 0.55). The PE score is 0.51 for H-85 and 0.45 for H-08MV, respectively. These PE scores imply that the empirical auroral models have considerable variance in their predictions. This conclusion is supported by the earlier work of *Gussenhoven et al.* (1983), which showed that the Hardy auroral boundary model has a standard deviation of about one degree for Kp < 3 and larger values for higher Kp (see Figure 3).

5. Conclusion

Auroral oval boundary has been considered a critical requirement for DMSP mission and space situational awareness. Auroral particle precipitation fluxes are essential environment data records acquired by DMSP satellites to meet the requirement. Both the equatorward and poleward boundaries of the auroral zone are the derived EDRs from particle flux data. The threshold requirement for auroral boundary is the identification of the auroral boundaries along the satellite path. Although both the equatorward and poleward boundaries are of interest, the equatorward boundary is of greater priority than the poleward boundary. Specification of the poleward boundary is usually considered as an objective requirement since its determination is often ambiguous.

The original Hardy auroral oval H-85 model has been extensively used for modeling high latitude phenomena and space weather operation since its initial development in 1985. The H-85 model gives the average spectra of particle fluxes from which mean values of various quantities like energy flux and mean energy are derived. One important objective of the model is to map the auroral boundary at all longitude for a given geomagnetic activity. The H-85 model has achieved a high level of maturity with explicit algorithms to predict auroral boundary location.

The H-85 model has recently been extended into a probability model H-08 with a much larger collection of new DMSP observations since 1985. Its improvement mitigates the H-85 deficiency by providing variance information. As a large database the upgraded Hardy H-08 model is nevertheless difficult to use and requires a functional representation. The present study has demonstrated a feasible approach to represent the H-08 model using real spherical harmonics functions. Briefly the functional representation we explored so far models only median energy flux and median energy. To expand utility of the H-08 model we are currently extending the present study to represent other model features. Further improvement will greatly enhance its usefulness for space weather prediction.

References

Gussenhoven, M. S., D. A. Hardy, and W. J. Burke, (1981), DMSP/F2 Electron Observations of Equatorward Auroral Boundaries and their Relationship to Magnetospheric Electric Fields, *J. Geophys. Res., 86*, pp. 768-778.

Gussenhoven, M. S., D. A. Hardy, and N. Heinemann, (1983), Systematics of the Equatorward Diffuse Auroral Boundary, *J. Geophys. Res., 88*, pp. 5692-5708.

Hardy, D. A., M. S. Gussenhoven, and E. Holeman, (1985), A Statistical Model of Auroral Electron Precipitation, *J. Geophys. Res., 90*, pp. 4229-4248.

Hardy, D. A., M. S. Gussenhoven, R.A. Raistrick, and W. McNeil, (1987), Statistical and Functional Representations of the Pattern of Auroral Energy Flux, Number Flux, and Conductivity, *J. Geophys. Res., 92*, pp. 12275-12294.

Hardy, D. A., E. G. Holeman, W. J. Burke, L. C. Gentile, and K. H. Bounar, (2008), Probability distributions of electron precipitation at high magnetic latitudes, *J. Geophys. Res*., 113, A06305, doi:10.1029/2007JA012746.

Hilmer. R., (2010), AF-GEOSPACE USER'S MANUAL VERSION 2.5 AND VERSION 2.5P, September 2010.

Lane, C. T., (2012), Comparative statistical analysis of auroral models, Air Force Institute of Technology, Master Thesis, AFIT/APPLPHY/ENP/12-M07.

Madden, D. and M. S. Gussenhoven, (1990), Auroral Boundary Index from 1983 to 1990, *GL-TR-90-0358*, Phillips Laboratory, Hanscom AFB, MA.

This page is intentionally left blank.

Appendix A. H-85 Model Regression Coefficients for the Equatorward Auroral Boundary

Table A-1. H-85 model regression coefficients for the equatorward auroral boundary Λ

$$\Lambda = \Lambda_o + \alpha K_p$$

MLT	Number*	Λ_o	α	CC†
0000-0100	17235	66.9	-1.79	-0.76
0100-0200	7234	66.7	-1.57	-0.70
0200-0300	8282	66.6	-1.64	-0.75
0300-0400	16153	67.0	-1.81	-0.78
0400-0500	35610	67.0	-1.88	-0.78
0500-0600	67812	67.7	-1.81	-0.78
0600-0700	72618	68.2	-1.71	-0.73
0700-0800	56758	68.8	-1.58	-0.69
0800-0900	65537	69.7	-1.46	-0.65
0900-1000	61515	70.0	-1.19	-0.53
1000-1100	31844	70.2	-0.85	-0.41
1100-1200	14340	70.2	-0.41	-0.22
1200-1300	7954	71.3	-0.21	-0.12
1300-1400	7390	73.1	-0.44	-0.23
1400-1500	8313	72.8	-0.62	-0.34
1500-1600	11733	73.4	-1.09	-0.59
1600-1700	26411	73.5	-1.38	-0.73
1700-1800	45591	72.6	-1.51	-0.76
1800-1900	61810	71.7	-1.66	-0.80
1900-2000	66432	71.0	-1.83	-0.82
2000-2100	79626	70.0	-1.81	-0.81
2100-2200	63606	69.2	-1.94	-0.82
2200-2300	44349	68.1	-1.92	-0.83
2300-2400	32577	67.2	-1.83	-0.81

*Number of boundaries used in each regression

†Correlation coefficient between Λ and Kp.

Source: AF-Geospace software (Hilmer, 2010).

Appendix B. Coefficients for the H-08 Model Boundary

Table B-1. Coefficients for the H-08 model low latitude boundary Λ_L in Equation (2)

Index	Kp=0	Kp=1	Kp=2	Kp=3	Kp=4	Kp=5	Kp=6
a_0	1.1758	1.1504	1.1271	1.1068	1.0800	1.0544	1.0378
a_1	-0.0222	-0.0484	-0.0554	-0.0744	-0.0851	-0.0800	-0.0915
b_1	-0.0114	-0.0255	-0.0383	-0.0388	-0.0275	-0.0216	-0.0176
a_2	-0.0114	-0.0204	-0.0145	-0.0097	-0.0020	0.0046	0.0130
b_2	-0.0067	-0.0080	0.0115	0.0011	0.0119	0.0175	0.0129
a_3	-0.0011	0.0023	0.0083	0.0049	0.0095	0.0094	-0.0013
b_3	0.0010	0.0009	-0.0013	-0.0020	-0.0077	-0.0039	-0.0049
a_4	0.0006	-0.0002	-0.0059	0.0007	-0.0037	-0.0067	-0.0013
b_4	-0.0013	-0.0027	0.0027	0.0013	0.0010	0.0038	0.0050

Table B-2. Coefficients for the H-08 high latitude boundary Λ_H in Equation (3)

Index	Kp=0	Kp=1	Kp=2	Kp=3	Kp=4	Kp=5	Kp=6
c_0	1.3860	1.3969	1.3890	1.3898	1.3911	1.3796	1.3867
c_1	-0.0829	-0.0538	-0.0398	-0.0174	-0.0018	0.0150	0.0125
d_1	0.0116	0.0222	0.0070	0.0140	0.0195	0.0315	0.0183
c_2	-0.0169	-0.0026	-0.0100	-0.0011	-0.0020	-0.0041	-0.0095
d_2	0.0051	-0.0038	-0.0027	0.0077	0.0104	0.0085	0.0217
c_3	0.0039	0.0060	-0.0009	-0.0009	-0.0015	-0.0095	-0.0076
d_3	-0.0022	-0.0107	0.0024	0.0012	-0.0098	0.0022	0.0024

Appendix C. Regression Coefficients for the H-08MV Model

Table C-1. Regression coefficients C_{lk} in Equation (5)

Index	Kp=0	Kp=1	Kp=2	Kp=3	Kp=4	Kp=5	Kp=6
C_{00}	2.5933e+01	2.6419e+01	2.7018e+01	2.7331e+01	2.7642e+01	2.7752e+01	2.7679e+01
C_{10}	4.2699e-02	2.9665e-02	9.6545e-02	2.3478e-01	3.9974e-01	5.9882e-01	8.1152e-01
C_{11}	2.9979e-01	2.7641e-01	4.1384e-01	4.2845e-01	3.7436e-01	2.9723e-01	3.7766e-01
C_{12}	-4.0271e-01	-6.1018e-01	-7.7352e-01	-7.9939e-01	-6.7944e-01	-5.0470e-01	-7.0573e-01
C_{20}	-4.7319e-01	-6.3424e-01	-8.3750e-01	-9.8990e-01	-1.0881e+00	-1.2260e+00	-1.2178e+00
C_{21}	-8.2667e-02	-4.6545e-02	1.7062e-02	-2.9322e-02	-1.5787e-01	-2.6405e-01	-1.1977e-01
C_{22}	-9.6017e-02	-1.0683e-01	-1.1731e-01	-2.3017e-02	1.0577e-01	-2.5746e-02	-1.3074e-01
C_{23}	-1.0602e-01	-1.7478e-01	-2.6656e-01	-4.6299e-01	-5.3215e-01	-5.0706e-01	-5.3579e-01
C_{24}	4.6688e-02	-7.0096e-02	2.5682e-03	-7.5863e-02	-7.7337e-02	-2.0728e-01	-2.8664e-01
C_{30}	4.1655e-01	4.8183e-01	5.0093e-01	5.0559e-01	5.0510e-01	4.6267e-01,	4.4003e-01,
C_{31}	7.8009e-02	1.0694e-01	6.5848e-02	7.7903e-02	1.2989e-01	1.6437e-01	8.4770e-02
C_{32}	8.7785e-02	9.9011e-02	1.3824e-01	1.5905e-01	1.2522e-01	5.0911e-02	3.5080e-02
C_{33}	-1.5315e-01	-1.4413e-01	-7.2309e-02	-7.5693e-03	8.6032e-02	-1.2168e-02	1.7777e-01
C_{34}	-8.7330e-03	2.9115e-01	2.0476e-01	2.6477e-01	1.5019e-01	2.5081e-01	2.4226e-01
C_{35}	-2.5404e-01	-2.8757e-01	-3.0073e-01	-1.9864e-01	-1.3104e-01	-1.5396e-01	-1.0487e-01
C_{36}	2.6598e-02	-1.1223e-01	-2.0551e-01	-4.0589e-01	-3.2158e-01	-2.0497e-01	-1.6785e-01
C_{40}	-7.0876e-02	-6.5799e-02	4.5761e-02	-5.5574e-02	-4.9123e-02	-9.5350e-02	-1.4024e-01
C_{41}	3.7265e-02	1.2984e-01	1.4247e-01	2.2153e-01	3.0379e-01	1.6304e-01	1.4159e-01
C_{42}	1.7147e-01	3.0712e-01	2.5850e-01	3.1306e-01	2.1320e-01	2.5894e-01	2.1720e-01
C_{43}	3.4809e-02	-6.3848e-02	5.2888e-03	5.0161e-02	2.1075e-01	1.6739e-01	1.5175e-01
C_{44}	1.6392e-02	-1.4506e-01	-3.8450e-03	7.3798e-03	-6.4012e-02	-3.6353e-03	-1.8067e-02
C_{45}	4.4232e-02	6.4640e-03	9.8167e-02	2.0145e-01	-2.6796e-04	1.2838e-01	-4.6818e-03
C_{46}	5.6995e-03	4.4981e-02	-7.7958e-02	-1.9563e-01	-1.7600e-01	-2.1337e-01	-2.3249e-01
C_{47}	4.9388e-02	2.8978e-02	8.2980e-02	5.1840e-02	2.7555e-02	5.6134e-02	5.5444e-02
C_{48}	-3.7796e-02	-1.0546e-02	-6.2586e-03	-4.8818e-02	-4.8359e-02	-7.6932e-03	-3.4973e-02

Note: Coefficient C_{lk} matches the sequence with real spherical harmonics y_{lk} in Appendix D.

Table C-2. Regression coefficients D_{lk} in Equation (6)

Index	Kp=0	Kp=1	Kp=2	Kp=3	Kp=4	Kp=5	Kp=6
D_{00}	-1.7300e+00	-1.4493e+00	-1.1307E+00	-8.9516E-01	-8.2792E-01	-8.8079E-01	-1.0317E+00
D_{10}	4.8954e-02	1.9877e-01	4.8066E-01	7.4207E-01	8.3337E-01	9.8394E-01	1.0719E+00
D_{11}	3.4805e-01	4.5990e-01	5.9400E-01	5.8077E-01	4.9866E-01	3.8492E-01	3.1449E-01
D_{12}	-4.7046e-01	-5.9127e-01	-5.1359E-01	-5.0540E-01	-4.6081E-01	-3.0305E-01	-3.4897E-01
D_{20}	-1.0936e+00	-1.1012e+00	-1.1802E+00	-1.1446E+00	-1.2044E+00	-1.1934E+00	-9.7272E-01
D_{21}	-1.7796e-01	-2.8930e-01	-1.1049E-01	-1.9860E-01	-2.8294E-01	-4.0946E-01	-2.5643E-01
D_{22}	2.4059e-02	7.9987e-02	-4.4199E-02	-7.7953E-02	-3.9396E-02	-4.6639E-02	-1.8697E-01
D_{23}	-9.4771e-02	-2.5964e-01	-3.7743E-01	-5.2293E-01	-5.0814E-01	-4.6820E-01	-3.7312E-01
D_{24}	-2.3983e-02	-6.5280e-02	-1.4453E-01	-2.5212E-01	-3.0463E-01	-3.5296E-01	-3.5772E-01
D_{30}	5.2075e-01	6.4961e-01	6.2316E-01	5.9178E-01	5.7904E-01	4.8779E-01	4.3183E-01
D_{31}	1.6378e-02	2.6462e-01	2.7206E-01	2.7523E-01	3.0326E-01	2.7434E-01	4.0121E-02
D_{32}	-7.0786e-02	-8.4989e-02	1.5623E-01	2.0750E-01	1.9372E-01	2.0480E-01	1.2278E-01
D_{33}	7.1226e-02	,-3.4012e-02	1.0322E-01	1.3190E-01	1.0930E-01	2.5162E-02	1.4691E-01
D_{34}	8.2478e-02	4.2146e-01	2.5173E-01	3.4261E-01	4.6852E-01	4.2942E-01	4.5759E-01
D_{35}	2.2487e-02	-6.4025e-03	-1.9770E-01	-1.4019E-01	-8.5956E-02	-9.2246E-02	-9.7751E-03
D_{36}	2.6611e-01	9.3448e-02	1.7421E-01	1.0094E-01	-6.5296E-03	-2.0879E-02	-9.0104E-02
D_{40}	2.4341e-01	1.4175e-01	1.4508E-01	4.3554E-02	5.3648E-02	3.2140E-02	-4.8405E-02
D_{41}	-5.0369e-02	4.7840e-02	4.5021E-02	2.9833E-02	7.5888E-04	-8.3912E-02	-4.6096E-02
D_{42}	4.7256e-02	1.5081e-01	1.1735E-01	1.6831E-01	1.4838E-01	2.1080E-01	1.2729E-01
D_{43}	-7.6145e-02	-3.0821e-02	-4.4963E-02	-2.2661E-02	1.6409E-03	8.4459E-02	3.7660E-03
D_{44}	4.6876e-02	-7.3577e-03	1.8354E-01	1.8351E-01	1.4177E-01	1.6503E-01	2.2308E-02
D_{45}	1.2508e-02	6.2900e-02	-1.1056E-02	2.1242E-02	-1.6333E-01	-5.7537E-02	-2.2938E-02
D_{46}	3.9841e-02	-2.1440e-02	-1.1262E-01	-1.6892E-01	-8.9952E-02	-1.5480E-01	-1.5214E-01
D_{47}	6.2767e-03	8.3762e-02	1.3513E-02	-5.9936E-02	-1.0670E-01	-9.8622E-02	-8.2133E-02
D_{48}	2.0683e-02	-6.3000e-02	-1.6166E-01	-1.4319E-01	-1.4308E-01	-8.8456E-02	5.9848E-03

Note: Coefficient $D_{l,k}$ matches the sequence with real spherical harmonics y_{lk} in Appendix D.

Appendix D. Formulas of Real Spherical Harmonics

The formulas of the real spherical harmonics $y_{lk}(\theta, \phi)$ used in this study are based on "Table of spherical harmonics" in www.wikipedia.org. These formulas that are related to the complex spherical harmonics $Y_{lm}(\theta, \phi)$ are expressed in the Cartesian coordinate (x, y, z, and r). We transform θ and ϕ to the Cartesian coordinate through the usual spherical-to-Cartesian coordinate transformation with $r = 1$:

$$x = r \sin\theta \cos\phi$$
$$y = r \sin\theta \sin\phi$$
$$z = r \cos\theta$$

Real spherical harmonics with $l = 0$ is:

$$y_{00} = \frac{1}{2}\sqrt{\frac{1}{\pi}}$$

Real spherical harmonics with $l = 1$ are:

$$y_{10} = \sqrt{\frac{3}{4\pi}} \cdot \frac{x}{r}$$
$$y_{11} = \sqrt{\frac{3}{4\pi}} \cdot \frac{y}{r}$$
$$y_{12} = \sqrt{\frac{3}{4\pi}} \cdot \frac{z}{r}$$

Real spherical harmonics with $l = 2$ are:

$$y_{20} = \frac{1}{4}\sqrt{\frac{5}{\pi}} \cdot \frac{-x^2 - y^2 + 2z^2}{r^2}$$
$$y_{21} = \frac{1}{2}\sqrt{\frac{15}{\pi}} \cdot \frac{yz}{r^2}$$
$$y_{22} = \frac{1}{2}\sqrt{\frac{15}{\pi}} \cdot \frac{zx}{r^2}$$
$$y_{23} = \frac{1}{2}\sqrt{\frac{15}{\pi}} \cdot \frac{xy}{r^2}$$
$$y_{24} = \frac{1}{4}\sqrt{\frac{15}{\pi}} \cdot \frac{x^2 - y^2}{r^2}$$

Real spherical harmonics with $l = 3$ are:

$$y_{30} = \frac{1}{4}\sqrt{\frac{7}{\pi}} \cdot \frac{z(2z^2 - 3x^2 - 3y^2)}{r^3}$$

$$y_{31} = \frac{1}{4}\sqrt{\frac{35}{2\pi}} \cdot \frac{(3x^2 - y^2)y}{r^3}$$

$$y_{32} = \frac{1}{4}\sqrt{\frac{35}{2\pi}} \cdot \frac{(x^2 - 3y^2)x}{r^3}$$

$$y_{33} = \frac{1}{4}\sqrt{\frac{105}{\pi}} \cdot \frac{(x^2 - y^2)z}{r^3}$$

$$y_{34} = \frac{1}{2}\sqrt{\frac{105}{\pi}} \cdot \frac{xyz}{r^3}$$

$$y_{35} = \frac{1}{4}\sqrt{\frac{21}{2\pi}} \cdot \frac{y(4z^2 - x^2 - y^2)}{r^3}$$

$$y_{36} = \frac{1}{4}\sqrt{\frac{21}{2\pi}} \cdot \frac{x(4z^2 - x^2 - y^2)}{r^3}$$

Real spherical harmonics with $l = 4$ are:

$$y_{40} = \frac{3}{16}\sqrt{\frac{1}{\pi}} \cdot \frac{(35z^4 - 30z^2r^2 - 3r^4)}{r^4}$$

$$y_{41} = \frac{3}{4}\sqrt{\frac{5}{2\pi}} \cdot \frac{xz(7z^2 - 3r^2)}{r^4}$$

$$y_{42} = \frac{3}{4}\sqrt{\frac{5}{2\pi}} \cdot \frac{yz(7z^2 - 3r^2)}{r^4}$$

$$y_{43} = \frac{3}{8}\sqrt{\frac{5}{\pi}} \cdot \frac{(x^2 - y^2)(7z^2 - 3r^2)}{r^4}$$

$$y_{44} = \frac{3}{4}\sqrt{\frac{5}{\pi}} \cdot \frac{xy(7z^2 - r^2)}{r^4}$$

$$y_{45} = \frac{3}{4}\sqrt{\frac{35}{2\pi}} \cdot \frac{(x^2 - 3y^2)xz}{r^4}$$

$$y_{46} = \frac{3}{4}\sqrt{\frac{35}{2\pi}} \cdot \frac{(3x^2 - y^2)yz}{r^4}$$

$$y_{47} = \frac{3}{16}\sqrt{\frac{35}{\pi}} \cdot \frac{x^2(x^2 - 3y^2) - y^2(3x^2 - y^2)}{r^4}$$

$$y_{48} = \frac{3}{4}\sqrt{\frac{35}{\pi}} \cdot \frac{xy(x^2 - y^2)}{r^4}$$

DISTRIBUTION LIST

DTIC/OCP 8725 John J. Kingman Rd, Suite 0944 Ft Belvoir, VA 22060-6218	1 cy
AFRL/RVIL Kirtland AFB, NM 87117-5776	2 cys
Official Record Copy AFRL/RVBX/Dr. Cassandra G. Fesen	1 cy